Ocean Dynamics (2006) 56: 284–294
DOI 10.1007/s10236-006-0063-4

Johan Christian Winterwerp · Zheng Bing Wang · Theo van der Kaaij · Kristof Verelst · Arnout Bijlsma · Youri Meersschaut · Marc Sas

Flow velocity profiles in the Lower Scheldt estuary

Received: 17 December 2004 / Accepted: 13 January 2006 / Published online: 17 March 2006

Abstract Recent acoustic Doppler current profiler (ADCP)-measurements in the Scheldt estuary near Antwerp, Belgium, revealed anomalous, i.e. anti-clockwise circulations in a left bend during the major part of the flood period; these circulations were established shortly after the turn of the tide. During ebb, anti-clockwise circulations persisted, as predicted by classical theory. These data were analysed with a 3D and a 1DV-model. The 3D simulations reveal that the anomalous circulations are found when salinity is included in the computations—without salinity "normal" circulations were found. From analytical and 1DV simulations, it is concluded that a longitudinal salinity gradient $\partial S/\partial x$ may induce a near-bed maximum in flow velocity reversing the direction of the secondary currents. The 1DV-model was then used to assess the contribution of various processes one by one. It was found that because of a reduction in vertical mixing, the vertical velocity profile is not at equilibrium during the first phase of accelerating tide, further enhancing the effects of $\partial S/\partial x$. A small vertical salinity gradient $\partial S/\partial z$ appeared to have a very large effect as the crosscurrents of the secondary circulations induced by $\partial S/\partial x$ became an order of larger magnitude. However, at the site under consideration, the effects of transverse salinity gradients, generated by differential advection in the river bend, were dominant: adverse directions of the secondary circulations were found even when the vertical velocity profile became more regular with a more or less logarithmic shape, i.e. when the effects of $\partial S/\partial x$ and $\partial S/\partial z$ did not play a dominant role anymore. It is argued that data on the secondary velocity structure, which can be measured easily owing to today's developments in ADCP equipment, may serve as an indicator for the accuracy at which the salinity field is computed with 3D numerical models. Moreover, the large effect of the salinity structure on the velocity field must have a large impact on the morphological development of estuaries, which should therefore be accounted for in morphological modelling studies.

Keywords River bends · Secondary currents · Gravitational circulation · Estuarine morphology

Responsible Editor: Alejandro Souza

J. C. Winterwerp (✉)
Delft University of Technology,
Environmental Fluid Mechanics,
P.O. Box 5048, Delft 2600 GA, The Netherlands
e-mail: h.winterwerp@citg.tudelft.nl

J. C. Winterwerp · Z. B. Wang ·
T. van der Kaaij · A. Bijlsma
WL|Delft Hydraulics,
P.O. Box, 177, Delft 2600 MH, The Netherlands
e-mail: theo.vdkaaij@wldelft.nl
e-mail: arnout.bijlsma@wldelft.nl

Z. B. Wang
Delft University of Technology, Hydraulic Engineering,
P.O. Box 5048, Delft 2600 GA, The Netherlands
e-mail: z.b.wang@wldelft.nl

K. Verelst
Flanders Hydraulics Research,
Berchemlei 115,
Antwerp 2140, Belgium
e-mail: kristof.verelst@lin.vlaanderen.be

Y. Meersschaut
Flanders Hydraulics Laboratory,
Berchemlei 115,
Antwerp 2140, Belgium
e-mail: Youri.Meersschaut@Lin.Vlaanderen.Be

M. Sas
IMDC, Wilrijkstraat 37-45,
Antwerp 2140, Belgium
e-mail: msa.imdc@technum.be

1 Introduction

The occurrence of secondary currents induced in river bends is a well-known and well-studied phenomenon. Anti-clockwise circulations (with longitudinal axis in streamwise direction), for instance, are induced in right

bends (in flow direction[1]), as elaborated by, e.g. Kalkwijk and Booij (1986). Such circulations, together with the larger flow velocities in the outer bend, cause pronounced asymmetric cross sections of river bends (Struiksma et al. 1985). Such secondary currents are sketched in Fig. 1 showing near-bed cross currents towards the inner bend and near-surface cross currents towards the outer bend. The occurrence of secondary currents in straight channels, induced by longitudinal salinity gradients, earth rotation and shear was treated by Valle-Levinson et al. (2003). However, the effects of earth rotation are relatively small in the case treated in this study, as discussed below, and are therefore omitted in this paper.

Acoustic Doppler current profiler (ADCP)-measurements in the Scheldt estuary near Antwerp, Belgium (e.g. Fig. 2) were carried out on June 5, 2002, and revealed anti-clockwise circulations in a left bend with a radius of about $R = 2.5$ km during the larger part of the flood period; these circulations were established shortly after the turn of the tide. This is depicted in Fig. 3, showing measured velocity vectors near the riverbed (red arrows) and near the water surface (blue arrows), and is further illustrated in Fig. 4 showing vertical profiles of velocity magnitude, direction and salinity at the same time as Fig. 3 for station D2. The vertical velocity profile shows a near-bed maximum, uncharacteristic for logarithmic velocity profiles in tidal (homogeneous) flow. The vertical salinity gradient is small, but important, as will be discussed later in this paper. During ebbing flow, the secondary currents behaved again as in upland rivers, i.e., an anti-clockwise circulation, but the crosscurrents were relatively small. The cause of this anomaly during flood must be sought (partly) in the velocity patterns generated by the longitudinal and traverse salinity gradients in this part of the estuary:

- Longitudinal salinity gradients may induce larger velocities in the lower part of the water column; as a result of which, vertical velocity profiles during flood are characterised by a near-bed maximum (note that the magnitude of the red near-bed velocity vectors in Fig. 3 is larger than that of the blue near-surface velocity vectors, as in Fig. 4). Hence, the larger momentum is found in the lower part of the water column and an anti-clockwise circulation is generated. During ebb, the salinity gradients work in the direction of the flow increasing the vertical velocity gradients, with a near-surface maximum.
- Transverse salinity gradients are generated through differential advection in the river bend, resulting in an uneven transverse salinity distribution. The salinity in the outer bend therefore tends to be smaller than in the thalweg, c.q. inner bend, both during the ebb and flood period. Hence, transverse salinity gradients are expected to generate an anti-clockwise secondary circulation during flood and a clockwise circulation during ebb, in a left bend.

Hence, during flood, longitudinal and transverse salinity gradients tend to strengthen each other in generating anti-clockwise circulations in a left bend, whereas during ebb, transverse salinity gradients tend to oppose the anti-clockwise circulations induced by the curvature of the flow, enhanced by longitudinal salinity gradients. Note that the Rossby number Ro (= U/fR, where U = mean flow velocity, f = Coriolis frequency and R = bend radius) in this part of the river amounts to about 3.5, so that Coriolis effects can be neglected to first order.

These observations were further confirmed in a hydrodynamic scale model of this stretch of the river in which the same circulation patterns were revealed (results are not presented here). Moreover, we have carried out three-dimensional numerical simulations of the water flow in the Scheldt estuary, the results of which are presented in Section 2.

The effects of horizontal salinity gradients on the vertical profile of the longitudinal velocity was studied for instance by Hansen and Rattray (1965) and Chatwin (1976). Prandle (1982) showed how near-bed and mid-depth maxima in the velocity profile around slack water are affected by viscosity. In particular, the analysis by Hansen and Rattray (1965) has received considerable attention as they provide a useful scheme classifying the stratification regime in estuaries.

The effect of horizontal salinity gradients (gravitational circulation) on secondary currents in estuaries through their effect on the vertical velocity profile was described in a clear, but qualitative way by Dyer (1977, 1997). Today's developments in measuring techniques (ADCP) and three-dimensional numerical modelling are so much more advanced than in the 1970s that we can quantify Dyer's analyses in more detail. For instance, Lacy and Monismith (2001) measured circulations in a curved stratified estuarine channel opposite to expected, during major parts of both the ebb and flood periods. The anomalous circulation during flood was attributed to a vertical velocity profile with near-bed maximum, which was reasoned to result from advection of low momentum inflow in the upper part of the water column. Reversal of the secondary current during part of the flood period and the anomalous circulation during the major part of the ebb period were attributed to lateral salinity gradients induced by differential advection.

Lateral salinity gradients, however, may augment, decrease, or reverse the direction of secondary circulations in channel bends, depending on the direction of these gradients (e.g. Geyer 1993; Dronkers 1996; and Chant and Wilson 1997). Moreover, vertical stratification may increase the magnitude of secondary currents, as shown by Geyer (1993) who measured enhanced near-surface flow velocities because of buoyancy-induced damping of vertical momentum exchange. Later, Chant (2002) found large variations in secondary circulation patterns with river

[1] We define our positive x-axis in up-estuary direction. In the remainder of this paper, the bend's orientation is defined with respect to this axis, independent of flow direction, i.e. always in flood direction.

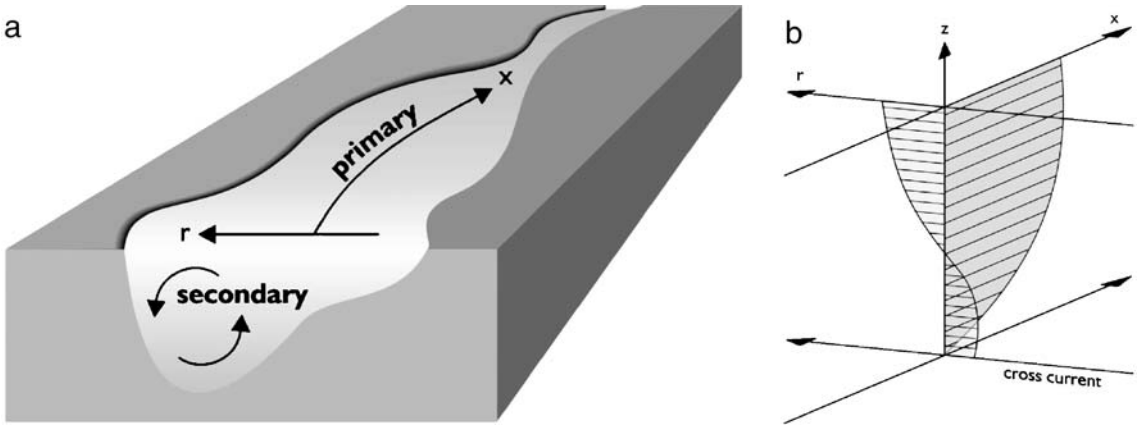

Fig. 1 Schematic river bend with secondary currents and definition of axes

run-off and over the spring-neap cycle from long-term ADCP-measurements in the New York harbour area. In particular, during high river flow and neap tide conditions, stratification effects became important inducing a two-cell secondary flow structure.

The conditions in the Scheldt estuary are such that salinity gradients are always present at the location of the new Deaurganckdok, the survey site discussed in this paper. This means we cannot wait for other conditions (tide, river runoff) and then measure the velocity structure in the absence of salt/brackish water, hence cannot test our hypothesis on the effect of salinity gradients on the direction of the secondary currents against field data in the Scheldt estuary. Fortunately, however, the progress in numerical modelling is such that today we can test our hypothesis with numerical simulations. First, we compare the velocity patterns computed with a full three-dimensional model with and without salinity. Then we strip the 3D model obtaining a 1DV POINT MODEL that we use to analyse the contribution of the various components of the salinity gradients. The results of the 3D and 1DV study are presented in Sections 2 and 3. Section 4 summarizes our main conclusions and presents a discussion on the implications of our findings to estuarine modelling.

2 3D numerical simulations of lower sea Scheldt

We have carried out homogeneous and inhomogeneous simulations (i.e. without and with salinity) for the survey

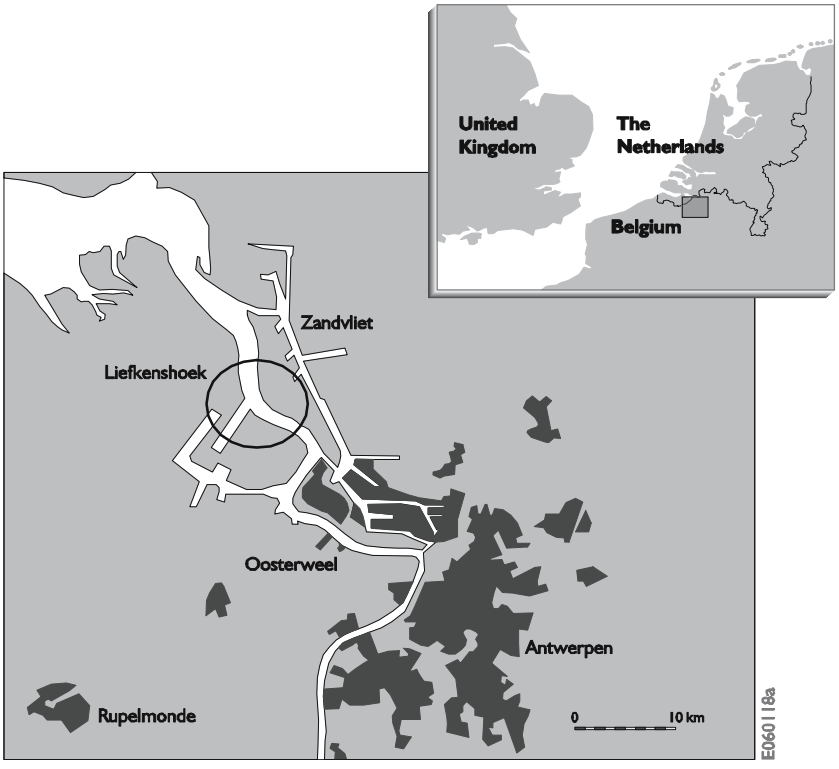

Fig. 2 The Lower Sea Scheldt estuary in Belgium with study area

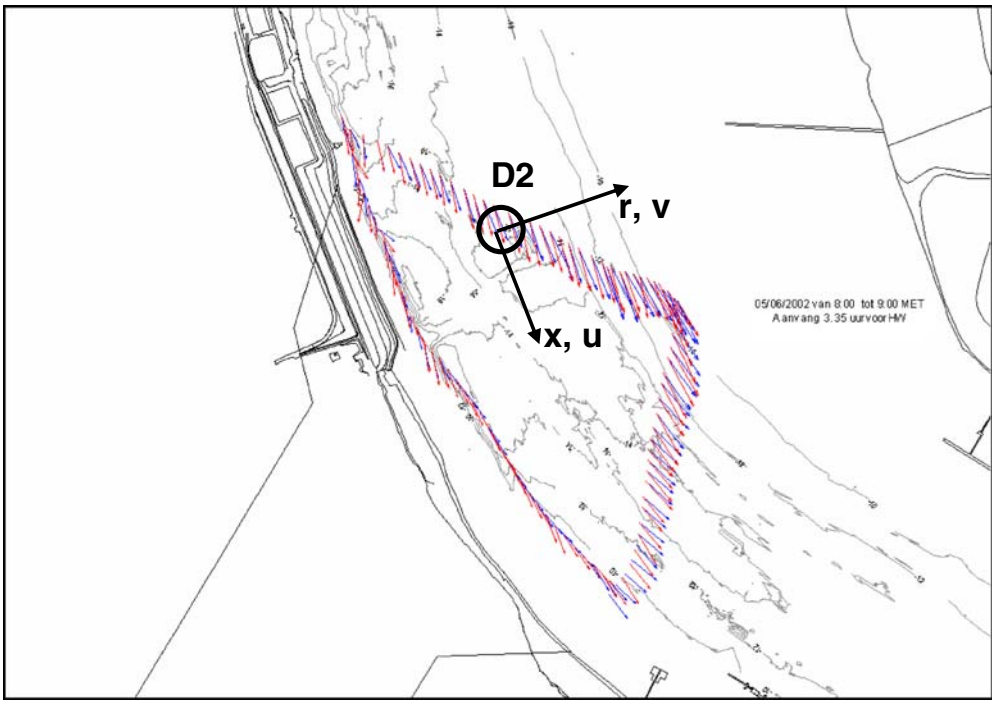

Fig. 3 ADCP measurements at 3:45 before HW showing anti-clockwise circulations; *red arrows* represent near-bed currents, whereas *blue arrows* represent near-surface currents

period (and a sufficient time before to spin up the model) with the software package DELFT3D (e.g. Lesser et al. 2004) to assess the effects of the salinity-induced density gradients on the velocity patterns in the Lower Sea Scheldt. The model consists of five separate computational domains running simultaneously whilst exchanging information on water levels, flow velocities and salinities, at the domain boundaries. In total, the curvilinear computational grid contains 27,500 computational cells. In the area of specific interest, grid cell sizes amount to approximately 25 m. The water column is schematised in ten sigma-layers with a relative thickness of 10% of the total (time-varying) water depth, amounting to 10–20 m in the river's channel.

The seaward boundary is situated at Waarde in the Western Scheldt, and the landward boundary at Rupelmonde, so that a domain of about 60 km length is covered. At the seaward boundary, a combination of water level and velocity time series is applied, and at the landward boundary a discharge time series. In addition, at both open boundaries, time-series of salinity are prescribed. The boundary conditions are generated with a 2Dh hydrodynamic model for the whole Scheldt estuary.

In horizontal direction, a constant horizontal eddy viscosity coefficient of 1 m^2/s is prescribed. The vertical eddy viscosity and diffusivity are computed with a k–ε-model. The bed roughness in the Lower Sea Scheldt is schematised by a constant Chézy-value of 70 $m^{1/2}/s$.

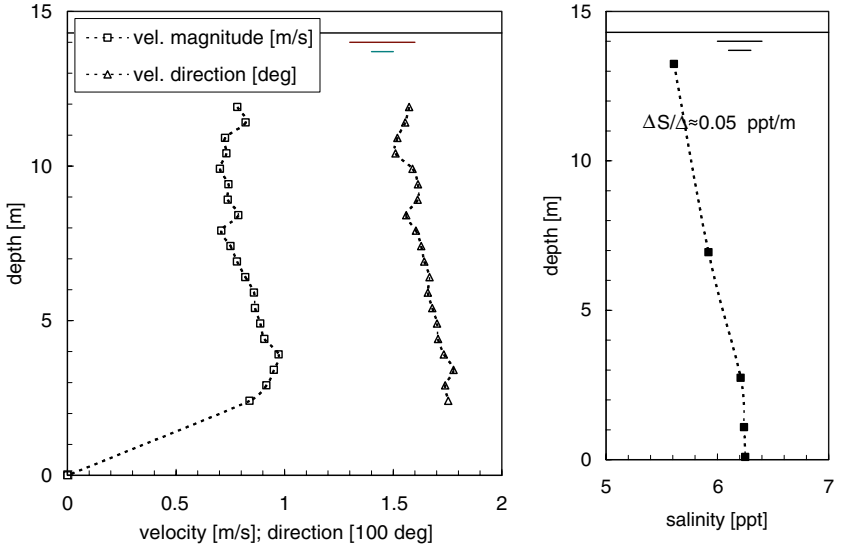

Fig. 4 Vertical profiles of velocity (*left panel*) and salinity (*right panel*) at station D2 in Lower Sea Scheldt (see Fig. 3)

Before applying the model, an extensive calibration was executed. Measured time series of water levels, flow rates and salinities were compared with computed time series. In addition, the measured exchange of water between a harbour basin (Kallo Dock) and the Lower Sea Scheldt was compared with the computed exchange. From those comparisons, it was concluded that the model was capable of properly reproducing the observed behaviour of hydrodynamics and salinity in the Lower Sea Scheldt.

Figure 5 shows computed vertical velocity profiles at station D2 (Fig. 3) during the first phase of the flood tide (t=19:00, 19:30, 20:00 and 20:30 h; low water slack at about t=18:45 h), both for homogeneous and inhomogeneous conditions. It is shown that during the first three times a pronounced near-bed to mid-depth maximum in velocity is found, whereas at t=20:30 h and beyond a more regular velocity profile is predicted. Figure 6 presents the computed vertical profiles of flow direction. In case of homogenous conditions, the profiles are slightly tilted to the right, implying weak clockwise circulations. For the inhomogeneous computations, the profiles are strongly skewed to the left in accordance with the strong anti-clockwise secondary flow depicted in Fig. 4. It is remarkable that also at t=21:30 h such an anti-clockwise circulation is found, whereas the velocity profile itself has attained an almost logarithmic shape (e.g. Fig. 5). This implies that probably the effects of the transverse salinity gradients dominate. This is further elaborated in Section 4.

Computed vector fields of the near-bed and near-surface flow field are presented in Fig. 7a,b for inhomogeneous and homogeneous conditions, respectively. For the homogeneous case (S=0), a regular clockwise circulation pattern in the river's left bend is found. However, for the inhomogeneous case, a pronounced anti-clockwise circulation is predicted (red arrows: near-bed currents, black arrows: near-surface currents). Comparison with Fig. 3 shows that the computed circulation pattern is in the same direction as the measured one, but much more pronounced. This is explained from a slight over-prediction of the vertical salinity gradients, computed with the numerical model, as can be seen from a comparison of the insert in Fig. 7a with Fig. 4b (see also Section 3).

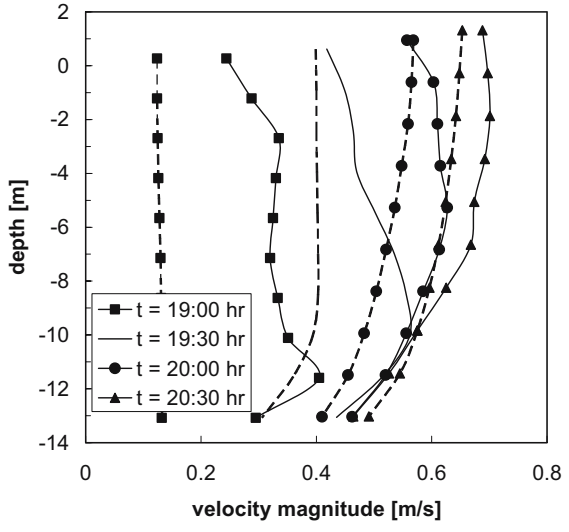

Fig. 5 Vertical velocity profiles computed at D2 with DELFT3D for t=19:00, 19:30, 20:00 and 20:30 h for homogeneous (*dashed line*) and inhomogeneous conditions (*solid line*)

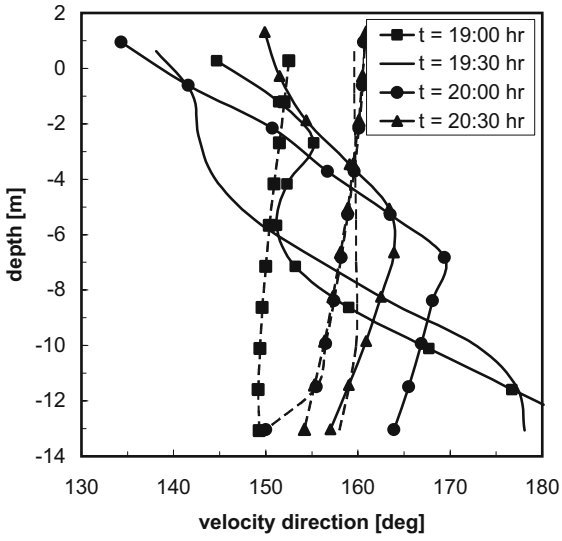

Fig. 6 Vertical profiles of flow direction computed at D2 (e.g. Fig. 3) with DELFT3D for t=19:00, 19:30, 20:00 and 20:30 h for homogeneous (*dashed line*) and inhomogeneous conditions (*solid line*)

The role of the vertical salinity gradients is further elaborated in the next section. Note that the computed mean longitudinal salinity gradient $\partial S/\partial x$ amounts to about $\partial S/\partial x = 0.3\,10^{-3}\,\mathrm{ppt/m}$, which is comparable to the measured values. It is noted that this gradient is considerably smaller than observations in most estuaries, where values of the longitudinal salinity gradient amount typically to $\partial S/\partial x = 10^{-3}\,\mathrm{ppt/m}$. However, this gradient is not constant over the water depth, but shows a pronounced maximum at mid-water depth (see insert Fig. 7). We elaborate on the role of vertical gradients on $\partial S/\partial x$ in Section 3 as well.

The three-dimensional simulations have shown that the observed near-bed maximum in flow velocity and anti-clockwise secondary currents are indeed predicted, though a bit exaggerated, by including salinity in the numerical model. In the next section, we investigate the effects of salinity further by analysing the various salinity contributions separately.

3 The vertical velocity profile as a function of salinity

Longitudinal salinity gradients generate a circulation pattern in the vertical plane, known as gravitational circulation with near-bed residual currents opposite to the direction of the salinity gradient. The induced vertical velocity profile has received considerable attention in literature. In particular, the classification scheme developed by Hansen and Rattray (1965) is to be mentioned as this

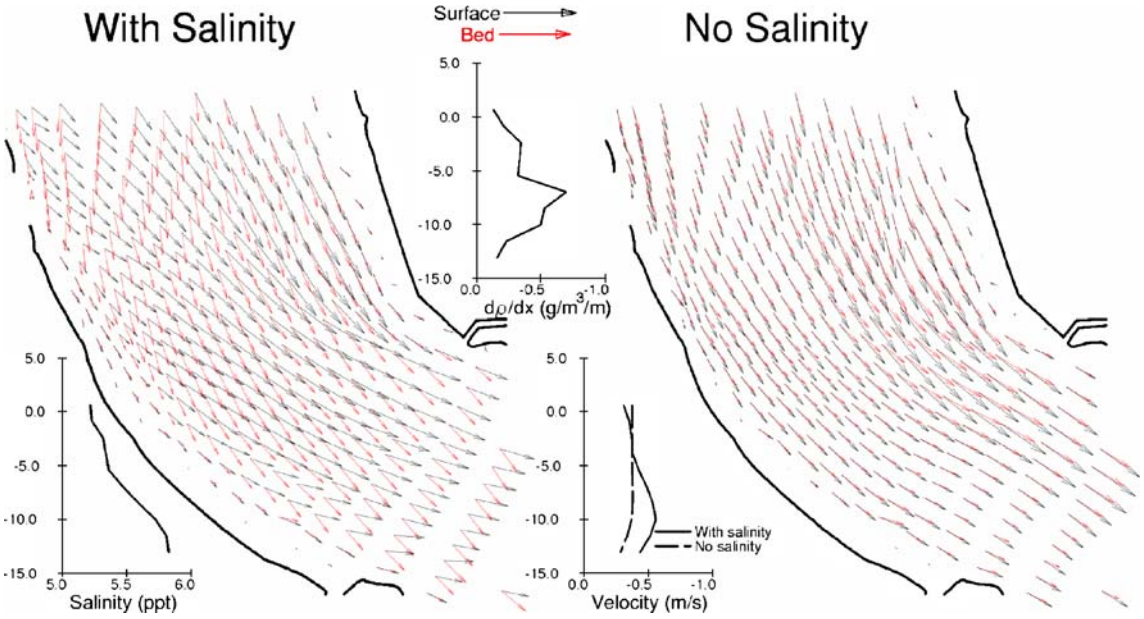

Fig. 7 Computed near-bed (*red arrows*) and near-surface (*black arrows*) velocity vectors for inhomogeneous conditions (*left panel*) and homogeneous conditions (*right panel*); t=19:30 h

provides a useful framework to analyse estuarine circulations. A further elaboration of this work was presented by Chatwin (1976). Van der Kreeke and Zimmerman (1990) have analysed the work carried out until that moment, distinguishing between a so-called diffusive and convective regime. In this paper, we focus on the convective regime, i.e. when gravitational effects govern the salinity distribution. The vertical velocity profile, as a function of salinity gradients, is computed with two methods:

1. We solve the momentum equation analytically, accounting for horizontal pressure gradients induced by surface slope and constant horizontal salinity gradient. We assume a parabolic vertical viscosity profile, as suggested by Kranenburg (1996), contrary to the approach by Hansen and Rattray (1965) and Chatwin (1976), who both used a constant vertical eddy viscosity.
2. We solve the momentum equation with the 1DV POINT MODEL applied in earlier hydro-sedimentological studies (Winterwerp 2001). Vertical mixing in this model is computed with the standard k–ε turbulence model, including the effects of buoyancy destruction by vertical salinity gradients. The 1DV-model is used to:
   - Compare the numerical solution with the analytical one,
   - Assess the effects of non-steady solutions, and
   - Assess the effects of vertical and transverse salinity gradients $\partial S/\partial z$ and $\partial S/\partial r$, respectively.

The one-dimensional horizontal momentum equation in main flow direction x reads:

$$\frac{\partial u}{\partial t}+\frac{1}{\rho}\frac{\partial p}{\partial x}+\frac{\partial \tau_{xz}}{\partial z}=0 \tag{1}$$

where $u(t,z)$ = longitudinal flow velocity (x–direction), p = pressure, ρ = water density, τ_{xz} = shear stress, t = time, and x and z are the co-ordinates in main current and vertical direction (e.g. Figs. 1 and 3), respectively, with z positive upward from the bed at z=0. We assume a hydrostatic pressure distribution $\partial p/\partial z=-g\rho$ and a linear vertical density profile:

$$\rho=\rho_0(1+(h-z)\beta)\ ;\ \beta=\frac{1}{\rho_0}\frac{\partial \rho}{\partial z}\neq\beta\{z\} \tag{2}$$

which is related to the vertical salinity profile $S(z)$ through a simplified equation of state:

$$\rho=\rho_f+\alpha S\ ;\ \alpha\approx 0.8 \tag{3}$$

in which ρ_f is the specific density of fresh water. The longitudinal pressure gradient for hydrostatic conditions is composed of a contribution by the surface slope and the density (c.q. salinity) gradients:

$$\begin{aligned}\frac{\partial p}{\partial x}&=g\rho_0\frac{\partial h}{\partial x}[1+\beta(h-z)]\\&\quad+g(h-z)\frac{\partial \rho}{\partial x}\left[1+\frac{1}{2}\beta(h-z)\right]\\&\approx g\rho\frac{\partial h}{\partial x}+g(h-z)\frac{\partial \rho}{\partial x}\end{aligned} \tag{4}$$

where h = water depth with respect to a horizontal datum (z=0) and g = acceleration of gravity. For most vertical salinity gradients observed in nature, $\beta(h\text{-}z)<<1$, as a result of which, we can ignore the contribution of the vertical salinity gradient to the longitudinal pressure gradient, as indicated in Eq. 4.

However, the effects of vertical salinity gradients on vertical mixing and on the vertical velocity profile are not negligible, as shown in our 1DV-analysis below. Inclusion in our analytical analysis is possible, but only at zero order, not affecting the vertical velocity profile. We therefore elaborate on vertical stratification effects in our numerical analyses only. In our analytical approach, we apply Fick's model and relate the shear stress to the velocity gradient through a parabolic eddy viscosity profile ν_z:

$$\nu_z = \kappa \frac{z}{h}(h-z)u_* \tag{5}$$

in which u_* = shear velocity and κ = Von Kármàn constant. If we apply a no-slip bed boundary condition (u=0 at z=z_0 with z_0 = roughness height) and τ_{xz}=p=0 at z=h, the steady-state solution to Eq. 1, using Eqs. 2, 3, 4 and 5 reads:

$$u(z) = -\frac{u_*}{\kappa}\ln\left\{\frac{z}{z_0}\right\} + \frac{1}{2}\frac{\alpha g h}{\kappa u_*}(z-z_0)\frac{1}{\rho}\frac{\partial S}{\partial x} \tag{6}$$

The first term of the right-hand side of Eq. 6 represents the familiar logarithmic velocity profile, and the second term accounts for the effect of the longitudinal salinity gradient on the velocity profile (baroclinic effects). The shear velocity u_* is still unknown. However, for given depth-averaged velocity U (i.e. given flow rate), $\partial S/\partial x$ and z_0, u_* can be expressed in these parameters. Integration of Eq. 6 over the water depth h yields a quadratic equation for u_*:

$$U = -\frac{u_*}{\kappa}\left[\ln\left\{\frac{h}{z_0}\right\} - 1\right] + \frac{1}{4}\frac{\alpha g h^2}{\kappa u_*}\frac{1}{\rho}\frac{\partial S}{\partial x} \tag{7}$$

from which u_* can be solved. For U=0.1 (0.1) 0.5 m/s, $\partial S/\partial x = 0.3\,10^{-3}\mathrm{ppt/m}$, h=10 m and z_0=1 mm, we present the corresponding vertical velocity profile in Fig. 8a.

Next, we solve the momentum in Eq. 1 with the 1DV POINT MODEL, in which we use a k–ε turbulence closure model, instead of the parabolic profile in Eq. 5 to establish ν_z, e.g. Winterwerp (2001). All 1DV-computations in this paper have been carried out with a 100-layer equidistant vertical resolution, unless stated differently; however, the results are not much different if we apply (much) less vertical resolution. The longitudinal pressure distribution in the model is prescribed such that the depth-averaged baroclinic effect is zero (see also Eq. 4):

$$\frac{1}{\rho}\frac{\partial p}{\partial x} = g\frac{\partial h}{\partial x} + \alpha g\left(z-\frac{h}{2}\right)\frac{1}{\rho}\frac{\partial S}{\partial x} \tag{8}$$

The magnitude and direction of the secondary currents in the river bend are computed from the momentum equation in radial direction r (e.g. Fig. 3), given the mean flow u computed above (e.g. De Vriend 1981 and Verbeek et al. 1999):

$$-\frac{u^2}{R} = -g\frac{\partial h}{\partial r} + \frac{\partial}{\partial z}\left(\nu_z\frac{\partial v}{\partial z}\right) - \alpha g(h-z)\frac{1}{\rho}\frac{\partial S}{\partial r} \tag{9}$$

in which R = bend radius and v = secondary velocity component, and in which we have accommodated for possible transverse salinity gradients. The secondary velocity component is defined as the velocity component perpendicular to the depth-mean velocity vector, and, by definition, its depth-mean value is zero. By integrating Eq. 9 over the water depth, and subtracting the results from Eq. 9, the transverse water slope can be eliminated:

$$-\frac{u^2-\overline{u^2}}{R} = \frac{\partial}{\partial z}\left(\nu_z\frac{\partial v}{\partial z}\right) + \frac{\tau_r}{\rho h} - \alpha g\left(\frac{h}{2}-z\right)\frac{1}{\rho}\frac{\partial S}{\partial r} \tag{10}$$

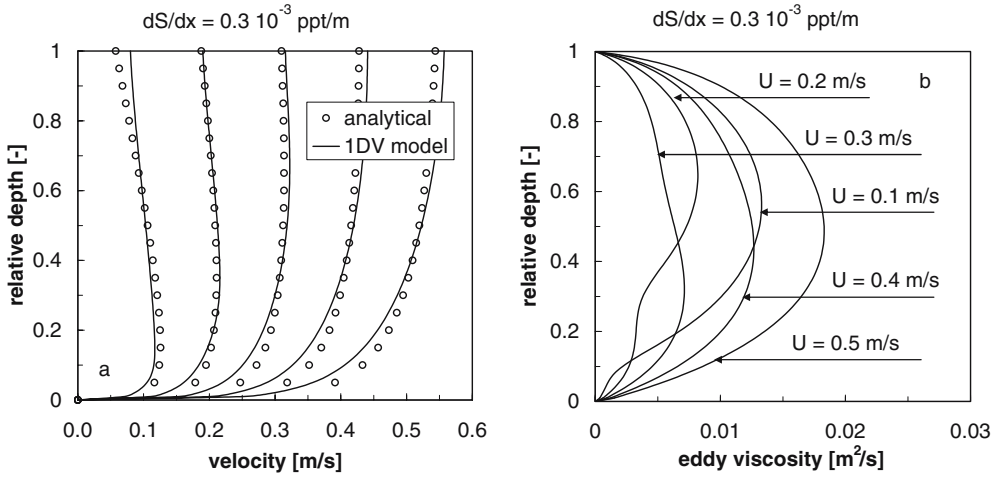

Fig. 8 **a** Vertical velocity profiles computed with Eq. 7 and 1DV-model; $\partial S/\partial z = 0$ for U=0.1 (0.1) 0.5 m/s. **b** Vertical eddy viscosity profiles computed with 1DV-model for U=0.1 (0.1) 0.5 m/s

where $\overline{u^2}$ =depth-averaged mean of u^2. Eq. 10 is solved off-line with the 1DV POINT MODEL, i.e. the secondary currents are assumed not to affect the main flow and/or the eddy viscosity profile. The bed shear stress in cross current direction is obtained by the requirement that the depth-mean value of v should be zero.

We have computed the vertical velocity profile for the same conditions as used for the analytical solution (i.e. steady state), and plotted the results in Fig. 8a as well. Note that in all our 1DV-simulations we prescribe the salinity gradients and keep these constant, hence, no mixing is accounted for. The horizontal salinity gradient is kept constant at the measured value, i.e. $\partial S/\partial x = 0.310^{-3}\,\mathrm{ppt/m}$.

Figure 8a shows that the analytical and 1DV numerical solutions do not match perfectly. The reason for these deviations much be sought wholly in the feedback between velocity profile (vertical shear) and eddy viscosity: the eddy viscosity profile $\nu_z(z)$ starts to deviate considerably from its parabolic shape because of chances in turbulence production induced by deviations of the velocity profile from its logarithmic shape, as shown by the computed $\nu_z(z)$ in Fig. 8b. Only at velocities beyond U=0.4 m/s, the 1DV viscosity profile re-establishes more or less its regular parabolic shape. For these conditions, a near-bed maximum in the velocity profile is found for $U \leq 0.4$ m/s.

The results presented in Fig. 8 have been obtained for stationary conditions to allow comparison with the analytical solution, i.e. U is set and kept constant at one of the specified values. Figure 9 presents the results of the 1DV computations in case of dynamic conditions, i.e. the depth-mean flow velocity U is varied sinusoidally with an amplitude of 1 m/s and period of 12.5 h, as in a tidal cycle. Figure 9a compares the velocity profiles computed for the dynamic and stationary case. Initially, i.e. up to U=0.5 m/s, the two cases show quite some difference; the dynamic case shows much more pronounced near-bed maxima in flow velocity, now up to U=0.4 m/s. For $U \geq 0.6$ m/s, the two cases overlap. Apparently, in the first part of the tidal cycle, the flow is not yet fully developed. This can be understood from an analysis of the computed eddy viscosity profiles. Initially, ν_z is quite small for the same reasons as above, i.e. small turbulence production because of small velocity gradients. This implies that the vertical mixing time, estimated by h^2/ν_z, then amounts to a few hours and equilibrium is only met when ν_z becomes large enough. In contrast, the stationary simulations are continued till equilibrium is found.

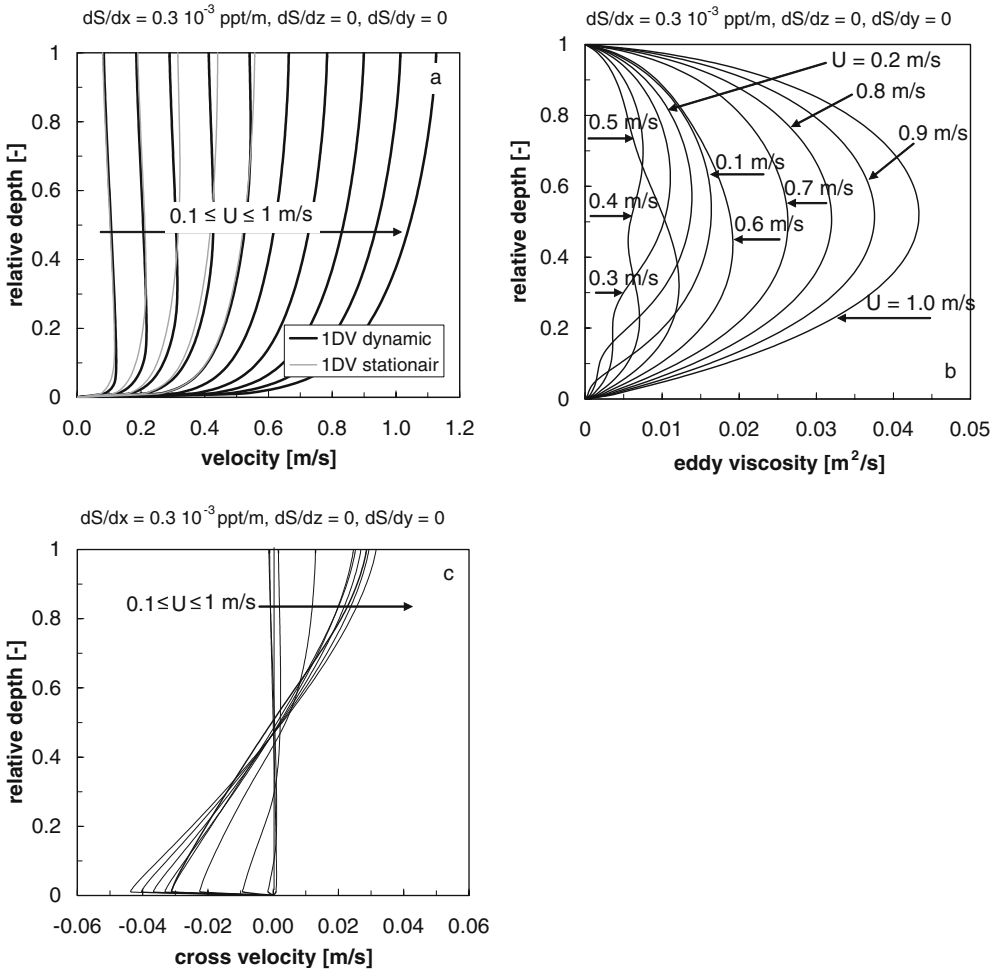

Fig. 9 Vertical profiles computed with 1DV-model for dynamic conditions with only longitudinal salinity gradient for U_{max}=1 m/s: **a** (*upper left panel*) longitudinal velocity; **b** (*upper right panel*) eddy viscosity; **c** (*left panel*) cross velocity (secondary current)

Figure 9c presents the computed secondary currents. It is shown that only for $U \leq 0.2$ m/s some adverse secondary currents are computed, but these are very small, i.e. of the order of a few mm/s only. At larger U, the expected secondary currents are computed (i.e. clockwise in a left bend) with near-bed maxima not exceeding 4.5 cm/s for U=1 m/s.

Next, we have introduced a small vertical salinity gradient as well, as was actually measured in the Scheldt estuary (Fig. 4). The 1DV results are presented in Fig. 10; again U is varied sinusoidally. Figure 10a shows that the effects of the salinity gradients are much larger now, in fact only for U=1 m/s, a more or less regular logarithmic velocity profile is re-attained. The near-bed maximum shifts upward with increasing U, as in the 3D simulations (Fig. 5). At U=0.5 m/s, the maximum in U is found more or less at mid-depth. It is noted that the vertical velocity profiles may seem a bit unrealistic with their pronounced kink. This is caused by the prescription of a rigid vertical salinity gradient—in reality there is feed-back between u, S (and $\partial S/\partial z$) and ν_z, which cannot be modelled in a 1DV model. For the smaller flow velocities, the eddy viscosity is now (Fig. 10b) almost an order of magnitude smaller than in Fig. 9b, which of course has to be attributed both to buoyancy induced damping by the vertical salinity profile and the maximum in the velocity profile (zero velocity gradient). The computed secondary are plotted in Fig. 10c, showing the reverse rotational direction up to U=0.5 m/s. In addition, the near-bed maximum in cross flow velocity is much larger now, up to 10 cm/s. It is remarkable that the computed cross currents for U=0.7 and 0.8 m/s are larger than those for U=0.9 and 1.0 m/s. This is an artefact of the 1DV approach due to the smaller mixing (ν_z) at U=0.7 and 0.8 m/s, as a result of which a kind of decoupling of the near-surface water is computed. In reality, there is a feed-back between the longitudinal and transverse currents—the computed large cross currents (and their vertical gradients) at U=0.7 and 0.8 m/s would induce stronger mixing, increasing ν_z, opposing the computed trend and stabilizing the vertical profile.

As expected, 1DV computations with $\partial S/\partial z$ only result in a 'laminarization' of the velocity profile induced by the vertical stratification. Hence, a longitudinal density gradient ($\partial S/\partial z$) is a necessary condition for the observed near-bed maximum in the velocity profile and the accompanied reverse secondary circulation, whereas the vertical stratification determines the magnitude of these effects. Of course, this is not a new observation, e.g. Dyer (1977).

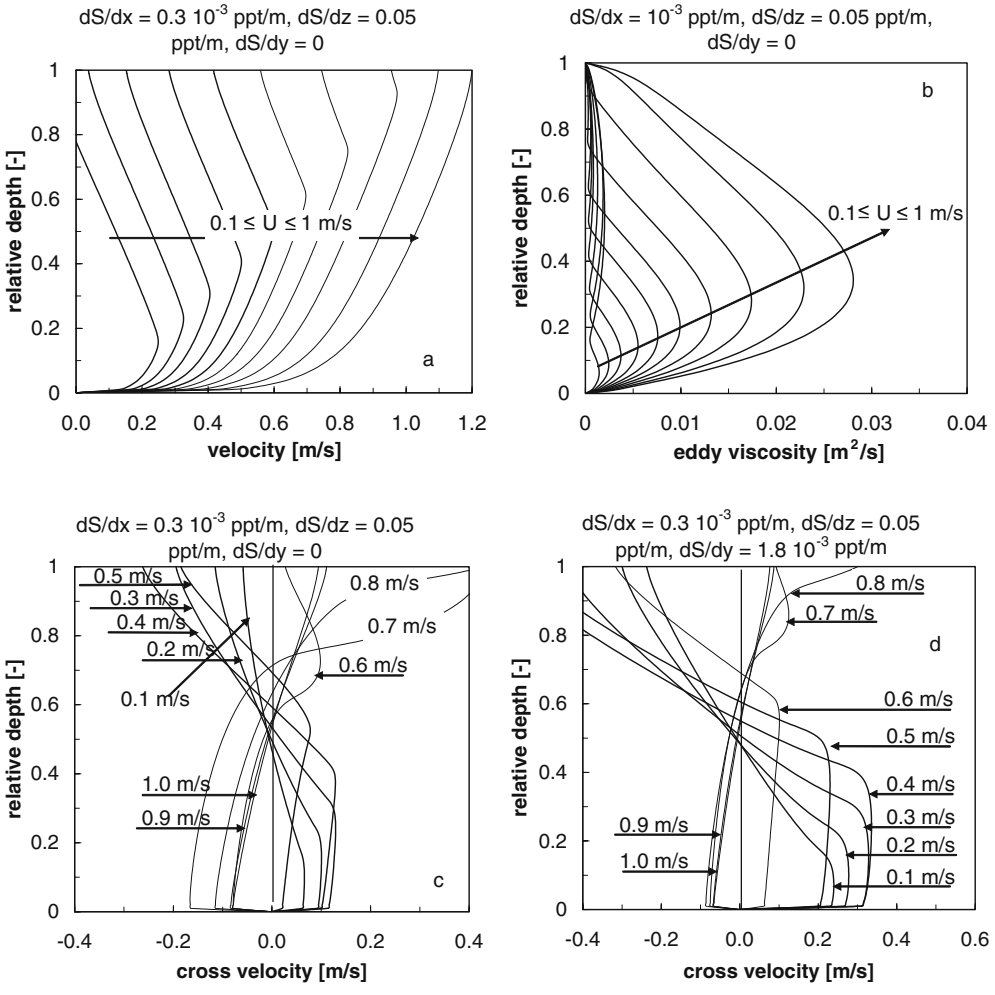

Fig. 10 Vertical profiles computed with 1DV-model for dynamic conditions with longitudinal and vertical salinity gradient for U_{max}=1 m/s: **a** (*upper left panel*) longitudinal velocity; **b** (*upper right panel*) eddy viscosity; **c** (*left panel*) cross velocity (secondary current); **d** (*right panel*) same as **c**, but with lateral salinity gradient

The results of the 3D computations (insert on Fig. 7) suggest that $\partial S/\partial x$ is not constant over the water depth. However, it is almost impossible to measure the vertical profile of $\partial S/\partial x$. Therefore, we applied the results of the 3D model to study the effect of this gradient on the velocity profile with the 1DV model. However, we do not present the results of these 1D simulations, as they hardly differ from the case with a constant $\partial S/\partial x$. This agrees with our analysis of Eq. 4 that, the contribution of vertical gradients in salinity on the effects of the longitudinal salinity (pressure) gradients is negligible.

Figure 10d presents the effects of a lateral salinity gradient $\partial S/\partial r$ on the secondary currents. As $\partial S/\partial r$ could not be measured, it is retrieved from the 3D computations, yielding $\partial S/\partial r \approx 0.8\ 10^{-3}$ ppt/m. Now we observe anti-clockwise circulations up to $U = 0.6$ m/s; moreover, the crosscurrents are much larger (compare with Fig. 10c). This suggests that for the case under consideration, the contribution by a transverse salinity gradient is larger than by the longitudinal and vertical salinity gradients. This finding is in agreement with our observation in Section 2 on the analysis of the 3D simulations.

4 Discussion and conclusions

Recent ADCP-measurements in the Scheldt estuary near Antwerp, Belgium, revealed anomalous, i.e. anti-clockwise circulations in a left bend during the major part of the flood period; these circulations were established shortly after the turn of the tide. During ebb, anti-clockwise circulations persisted, as predicted by classical theory. These data were analysed with a 3D and a 1DV-model. Both the 3D and the 1DV computations suggest a strong influence of the transverse salinity gradients. These observations can be sustained further from an analysis of the magnitude of the first and fourth term of Eq. 10. The transverse salinity gradient $\partial S/\partial r$ is a function of the local flow velocity u, the longitudinal salinity gradient $\partial S/\partial x$, and the local bathymetry, i.e. bend curvature and cross section. However, it is not possible to derive a simple general expression of $\partial S/\partial r = F\{u, \partial S/\partial x, R, h(x,y)\}$ because of the large influence of the local bathymetry. Therefore, we have to use the values computed with the 3D model in our analysis. From this, we find $u^2 - \overline{u^2} \approx 0.1\overline{u^2} \approx 0.025\ \mathrm{m}^2/s^2$, $R = 2{,}500$ m, $\alpha = 0.8$, $g = 9.81$ m/s^2, $(h/2-z) \approx h/2 \approx 7$ m, $\rho = 1{,}005$ kg/m^3 and $\partial S/\partial r = 0.8\ 10^{-3}$ ppt/m. In that case, term 1 amounts to about 10^{-5} m/s^2, whereas term 4 amounts to about $4{\cdot}10^{-5}$ m/s^2. Hence, we conclude that the effects of transverse circulations dominate indeed in this case, as inferred in Sections 2 and 3.

From our 1DV analysis we conclude that a baroclinic effect (i.e. a longitudinal salinity gradient) can reverse the direction of secondary currents and that this effect is enhanced by a reduction in vertical mixing as a result of a reduction in turbulence production induced by the shape of the vertical velocity profile. This also explains why small vertical gradients in the salinity structure have such a large effect on the magnitude of the secondary currents. For the conditions in the Lower Scheldt estuary under the current conditions, the transverse salinity gradient is apparently the larger one. However, the relatively large longitudinal flow velocities near the bed can only be explained from the horizontal and vertical salinity gradients.

It is further noted that the 1DV analysis can only be interpreted in a qualitative way as we have decoupled the contribution of the vertical velocity and salinity profiles induced by $\partial S/\partial x$ and $\partial S/\partial z$, from the ones induced by $\partial S/\partial r$. Moreover, vertical and transverse salinity gradients are not constant in time, but vary considerably from slack water to maximum ebb and flood velocity. This is probably (one of) the reason(s) that we were not able to reproduce the measured data (Fig. 4) on vertical and transverse flow structure with our 1DV model. Moreover, in wider estuaries, and when stratification becomes more pronounced, the effects of earth rotation may become important as well, complicating the analyses further.

A general conclusion of this study is that longitudinal and transverse velocity profiles are very sensitive to the salinity structure, and that even very small vertical salinity gradients can have a very large effect, in particular, on the secondary circulations. However, it is not yet possible to measure the salinity structure at the accuracy and resolution now possible for the flow field, where ADCP deployment yield detailed space- and time-covering information. As a result, data for calibrating 3D numerical models with respect to salinity are incomplete, at best. However, the analysis in this paper suggests that the structure of the flow field may be used as an indicator whether the salinity field is simulated accurately enough. In the 3D simulations presented in this study, the vertical salinity gradients are over-predicted, resulting in some over-prediction of the secondary currents in the river bend(s) of the Lower Scheldt estuary.

A second general comment concerns the long-term impact of the flow structure in general and of the secondary currents in particular. These determine the morphodynamic developments of river bends to a large extend. A proper morphological model should therefore account for a proper modelling of the secondary currents, hence the salinity field to enable proper prediction of such developments. To the knowledge of the authors, this has not yet been of great priority to morphodynamic modellers. Finally, it is noted that in homogeneous estuaries, secondary currents during ebb and flood generate near-bed crosscurrents in the same direction (i.e. towards the inner bend), whereas in inhomogeneous estuaries the direction of the crosscurrent may reverse, as shown in this paper. This must have a considerable impact on the morphodynamic development of the cross section; indeed the bed in the river bend under consideration is fairly horizontal, not showing the very deep outer bend and shallow inner bend, as would be expected in a bend of such small radius.

Acknowledgement We would like to thank "Het Ministerie van de Vlaamse Gemeenschap" (Ministry of the Flemish Community) for financing this study and their approval to publish the results.

References

Chatwin PC (1976) Some remarks on the maintenance of the salinity distribution in estuaries. Estuar Coast Mar Sci 4:555–566

Chant RJ (2002) Secondary circulation in a region of flow curvature: relationship with tidal forcing and river discharge. J Geophys Res 107(C9):14/1–14/11

Chant RJ, Wilson RE (1997) Secondary circulation in a highly stratified estuary. J Geophys Res 102(C10):23,207–23,215

De Vriend HJ (1981) Steady flow in shallow channel bends, Ph.D. Thesis, Delft University of Technology

Dronkers J (1996) The influence of buoyancy on traverse circulation and on estuarine dynamics. In: Aubrey DG, Friedrichs CT (eds) Buoyancy effects on coastal and estuarine dynamics. AGU, Washington, pp 341–356

Dyer KR (1977) Lateral circulation effects in estuaries, in: estuaries, geophysics and the environment. National Academy of Sciences, Washington 2:22–29

Dyer KR (1997) Estuaries—a physical introduction. Wiley, Chisester

Geyer WR (1993) Three-dimensional tidal flow around headlands. J Geophys Res 98(C1):955–966

Hansen DV, Rattray M (1965) Gravitational circulation in straits and estuaries. J Mar Res 23(2):1–4–122

Kalkwijk JPTh, Booij R (1986) Adaptation of secondary flow in nearly horizontal flow. J Hydraul Res 24(1):19–37

Kranenburg C (1996) Density currents, course notes b81. Delft University of Technology, Faculty of Civil Engineering and Geosciences, The Netherlands

Lacy JR, Monismith SG (2001) Secondary currents in a curved, stratified, estuarine channel. J Geophys Res 106(C12):31, 283–31,302

Lesser GR, Roelvink JA, van Kester JATM, Stelling GS (2004) Development and validation of a three-dimensional morphological model. Coast Eng 51(8–9):883–915

Prandle D (1982) The vertical structure of tidal currents and other oscillatory flows. Cont Shelf Res 1(2):191–207

Struiksma N, Olesen KW, Flokstra C, De Vriend HJ (1985) Bed deformation in curved alluvial channels. J Hydraul Res 23 (1):57–79

Valle-Levinson A, Reyes C, Sanay R (2003) Effects of bathymetry, friction and rotation on estuary-ocean mixing. J Phys Oceanogr 33(11):2375–2393

Van de Kreeke J, Zimmerman JTF (1990) Gravitational circulation in well- and partially-mixed estuaries, in Ocean Engineering Science. In: Le Méhauté B, Hanes DM (eds) The Sea. Wiley–Interscience, New York 14(A):495–521

Verbeek H, Wang ZB, Thoolen PMC (1999) Secondary currents in estuarine morphodynamic modeling, a case-study of the Western Scheldt, IAHR symposium on river, coastal and estuarine morphodynamics, Genova, 1999, pp 649–658

Winterwerp JC (2001) Stratification effects by cohesive and non-cohesive sediment. J Geophys Res 106(C10):22,559–22,574